# MEASUREMENT OF MASS ATTENUATION COEFFICIENTS OF NIOBIUM, MOLYBDENUM, TANTALUM AND TUNGSTEN NEAR THE ABSORPTION EDGE

by

***Zhen WANG, Siming GUO*, Ziyao SHU, Xing ZHOU, Zhiwei LI, Shikui HUANG, and Jinjie WU****

National Institute of Metrology, China, Beijing

Scientific paper
https://doi.org/10.2298/NTRP2402111W

**This study utilizes the monochromatic X-ray radiation device established by the National Institute of Metrology, China, to conduct a systematic experimental investigation of the mass attenuation coefficients of niobium, molybdenum, tantalum, and tungsten metals near their K absorption edges. The device's ability to generate continuously tunable monochromatic X-rays and accurately measure photon counts provides an ideal condition for precise mass attenuation coefficient measurements. This study employs a minimum energy step of 0.1 keV to systematically obtain the jump ratio rK and jump factor JK near the K-absorption edges of the four materials. The experimental measurements are compared with theoretical values from NIST-XCOM, NIST-FFAST, and Phy-x databases, demonstrating a consistent trend between the experimental and theoretical results, with relative deviations within acceptable limits, thereby validating the reliability of the theoretical models. An uncertainty analysis reveals a combined relative uncertainty of less than 2.7 %, indicating that the experimental results and theoretical values are in good agreement, with deviations and uncertainties within acceptable ranges. This research provides important experimental data and theoretical references for the application of monochromatic X-ray radiation devices in the field of mass attenuation coefficient measurements.**

*Key words: mass attenuation coefficient, absorption edge, monochromatic X-ray, jump ratio, jump factor*

## INTRODUCTION

Interaction coefficients have significant application value in all practical problems involving ionizing radiation, among which the mass attenuation coefficient is a fundamental parameter needed to determine the penetration of X-rays and gamma rays in matter [1]. It has been widely used in radiation protection, medical imaging, industrial radiation detection, and material analysis. In the field of radiation protection, the selection of materials with different K-absorption edge characteristics for different energy ranges of rays can better shield ray energy, enhance the absorption of specific energy rays, and weaken the influence of weak absorption regions [2, 3]. In medical imaging, understanding the mass attenuation coefficient of different materials is important for optimizing imaging parameters and image quality [4, 5]. In the fields of industrial radiation detection and material analysis, the mass attenuation coefficient can be used to determine the composition and structure of materials [6]. The attenuation-related parameters depend on the photon energy and material content [7]. In addition, these parameters can be determined experimentally and theoretically [8, 9]. The interest in the K-edge energy region attenuation coefficient is due to the importance of absorption jump factors and jump ratios in many scientific application fields, such as cancer treatment, industrial radiation treatment, dosimetry calculations, radiation shielding, and X-ray fluorescence surface analysis [10, 11].

Radiation shielding can be optimized by selecting materials that possess distinct K-absorption edges, tailored to counteract various energy ranges of ray emissions. [12]. The K-edge effect enhances the absorption capacity for specific energy rays and can also weaken the influence of weak absorption regions [13]. In the past, researchers usually used radioactive isotope sources to measure the mass attenuation coefficient of different materials at different photon energies [14]. However, due to the discrete energy characteris-

* Corresponding authors, e-mails: gsm@nim.ac.cn
wujj@nim.ac.cn

tics of radioactive isotope sources, their ability to measure absorption edges is limited [15, 16]. In order to better understand the interaction between X-rays and matter, continuous and accurate measurements are required [17, 18]. In recent years, with the development of monochromatic X-ray source technology, people have been able to obtain continuous tunable and highly stable monochromatic X-rays, making it possible to accurately measure the mass attenuation coefficient [19, 20]. In 2016, the French National Laboratory (Laboratoire National Henri Becquerel, LNHB) and the German Physical Technical Institute (Physikalisch-Technische Bundesanstalt, PTB) cooperated to measure the mass attenuation coefficient of Cu and Zn with high accuracy, covering the mass attenuation coefficient range of K- and L-absorption edges [21, 22]. At the same time, the LNHB laboratory measured the attenuation coefficients of elements of interest and compared the obtained values with those used in the calculation code, possibly integrating them into MACAO [23, 24].

However, the current literature does not provide experimental results for materials such as niobium (Nb) and molybdenum (Mo), and experimental data for tantalum (Ta), and tungsten (W) in the continuous energy range are also blank. This paper uses a single-energy X-ray device with continuously tunable energy and measurable photon number to study the measurement of the mass attenuation coefficient of materials using gamma or X-ray attenuation. The K-edge jump ratio and jump factor were also calculated. Materials (Nb, Mo, Ta, W) were tested with a minimum 0.1 keV step near the K-edge. The experimental results were compared with Geant4 simulation results and theoretical calculations of NIST-XCOM, Phy-X, and NIST-FFAST.

## EXPERIMENTAL EQUIPMENT AND METHOD

### Experimental equipment

The LiF220 and LiF200 crystals are both forms of lithium fluoride and play crucial roles in the field of X-ray optics, particularly in the generation of monochromatic X-rays in the 8-40 keV energy range [25, 26]. Utilized as spectral dispersion media in monochromatic X-ray generation devices, these crystals harness the Bragg diffraction effect to disperse the broad-spectrum X-ray beam into X-rays of specific wavelengths [27, 28]. Monochromatic X-rays of this nature are of paramount importance in various fields, including material science analysis, medical imaging technology, and fundamental physics research, as they facilitate more precise data interpretation and image resolution [29, 30]. The selection of LiF220 and LiF200 crystals as spectral components is thereby intended to fulfill the demand for high-precision X-ray spectral analysis in these domains [31, 32].

To accurately measure the mass attenuation coefficient, this study utilized two single-color X-ray sources with different energy ranges: low energy and high energy. The low energy device utilized an X-ray machine to generate X-rays that were monochromatized by a LiF200 or LiF220 crystal, producing monochromatic X-rays within the 8-40 keV energy range. The high energy device used a Si220 crystal double monochromator to generate monochromatic X-rays in the 40-80 keV energy range. These crystals utilized the Bragg diffraction principle, where when the incident X-rays met the crystal at the Bragg angle, diffraction occurred, producing monochromatic X-rays. By adjusting the incident ray angle with the crystal, monochromatic X-rays within the corresponding energy range could be obtained. Both devices had good monochromaticity and stability, meeting the requirements for high-quality mass attenuation coefficient measurements.

The schematic diagram of the experimental measurement apparatus for the low energy section of the single-energy X-ray is shown in fig. 1. The monochromaticity of this device was better than 3 % at 10 keV, and the stability was better than 0.2 % within 4 hours [33, 34]. The single-energy beam was generated by the X-ray machine through bremsstrahlung radiation, which was then monochromatized by the LiF200 or LiF220 crystal to produce 8-40 keV single-energy X-rays. A posterior collimator and a limiting aperture were used behind the crystal to collimate the incident and transmitted beams to a 4 mm diameter. Overall, spatial scattering of X-rays was shielded, allowing the test system to meet the measurement requirements of *single-energy* and *narrow beam* energy spectra. The lead shielding plate placed in front of the materials and detectors effectively blocked scattered photons from affecting the experiment [35]. The measurement time was determined based on extensive previous experiments and was set to 200 seconds. At a given single-energy X-ray energy, the sample was placed on the path of the single-energy X-ray beam. A transverse moving guide rail was used to move the material foil, reducing the beam instability and human interference caused by switching on and off the X-ray machine. Finally, a high-resolution HPGe detector was used to measure the number of photons transmitted through different sample materials.

For the high energy section of the single-energy X-ray, the experimental measurement apparatus is illustrated in fig. 2. The X-ray machine was surrounded by a 7 mm thick lead shielding box to reduce X-ray scattering, resulting in stability better than 1 %. The mechanism for generating the single-energy beam was similar to the low energy section, but the crystal material used was a pair of parallel crystal faces with Si220 and a high-precision crystal adjustment bracket, producing 40-80 keV single-energy X-rays. In terms of

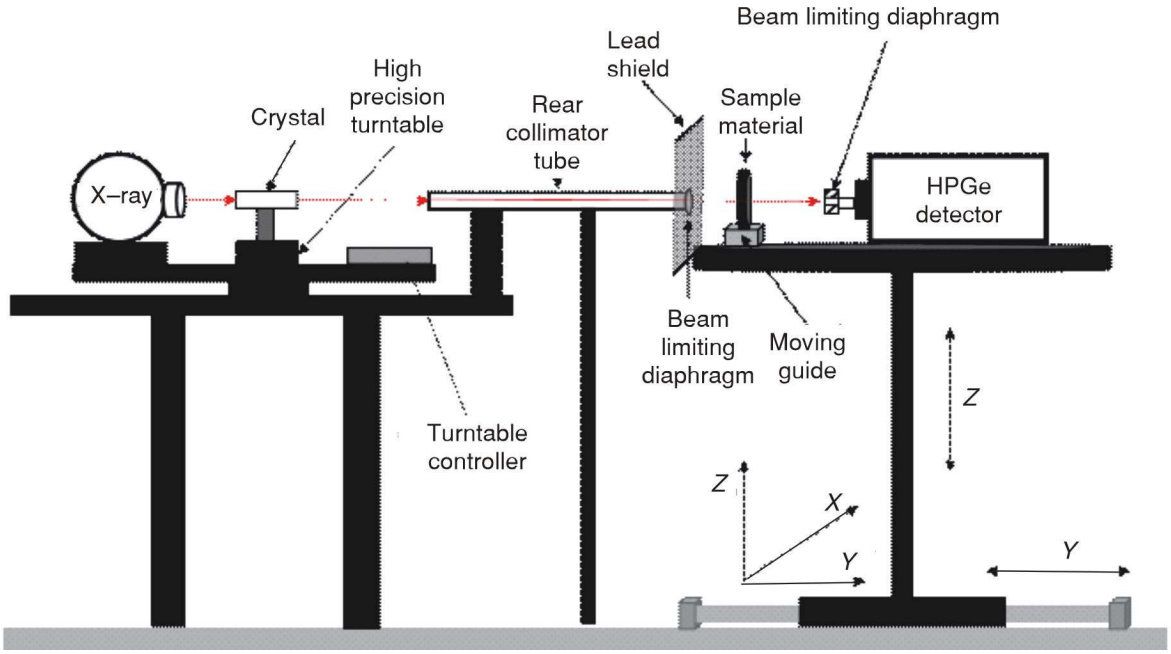


**Figure 1. Schematic diagram of low-energy experimental measurement device**

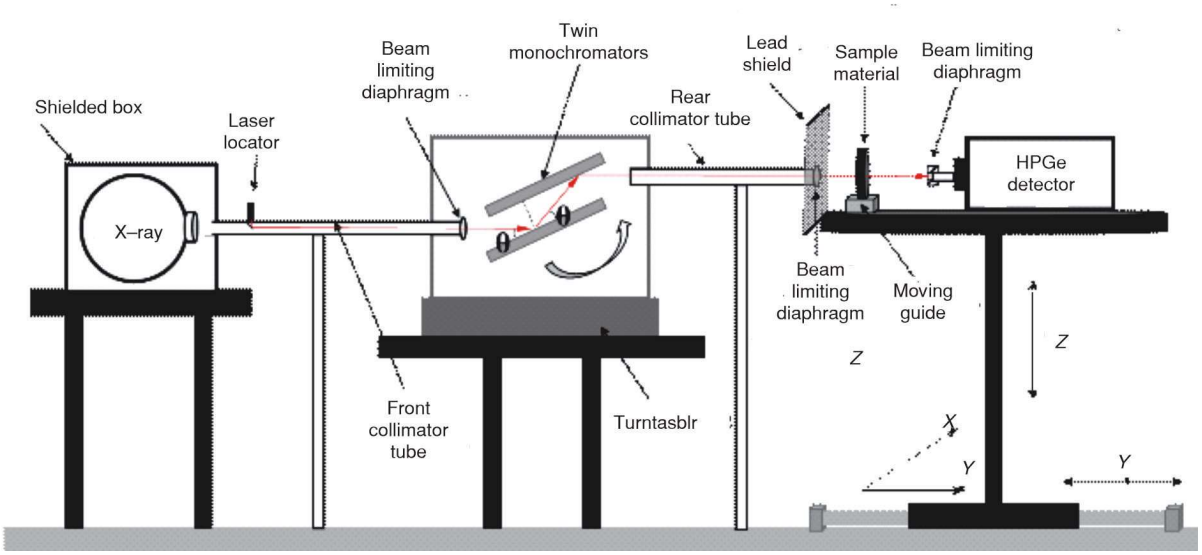


**Figure 2. Schematic diagram of the experimental measurement device for energy section**

beam flux, the photon flux of the monochromatic X-ray beam obtained by the double crystal monochromator was lower than that of the single crystal monochromator due to the twice Bragg diffraction. The beam stability was better than 0.26 %, with a maximum relative deviation of 0.02 % between the maximum and minimum energy points, demonstrating good overall energy stability. The monochromaticity of the device was better than 2.3 % [36].

In the selection of experimental samples, Nb and Mo metal foils were used for the low energy device measurement, while Ta and W metal foils were used for the high energy device measurement. These samples were of high purity, and their dimensions and thickness were measured to ensure the reliability of the experimental results, as shown in tab. 1.

## Experimental method

To ensure the accuracy of experimental data, it is imperative to calibrate the energy linearity of the High-Purity Germanium (HPGe) detector. This research undertaking involves the use of radioactive isotope standard point sources, including $^{57}$Co, $^{241}$Am, $^{152}$Eu, and $^{109}$Cd, for the calibration process. The procedure begins by measuring the energy spectra of these standard sources with the HPGe detector, fol-

**Table 1. The material parameters of sample material**

| Sample | Purity (mass fraction) [%] | Density [gcm$^{-3}$] | Nominal thickness [mm] | Quality [g] | Dimensions [mm] |
|---|---|---|---|---|---|
| Nb | 99.99 | 8.57 | 0.025 | 0.9 | φ80×80×0.025 |
| Mo | 99.99 | 10.2 | 0.03 | 1.502 | φ80×80×0.03 |
| Ta | 99.99 | 16.6 | 0.02 | 1.712 | φ80×80×0.02 |
| W | 99.99 | 19.3 | 0.05 | 4.798 | φ80×80×0.05 |

**Table 2. The relationship between energy and channel**

| Radionuclide | Energy [keV] | Channel |
|---|---|---|
| $^{57}$Co | 6.404 | 149 |
| | 14.413 | 335 |
| $^{241}$Am | 13.944 | 324 |
| | 59.541 | 1388 |
| $^{152}$Eu | 45.289 | 1057 |
| $^{109}$Cd | 22.163 | 516 |

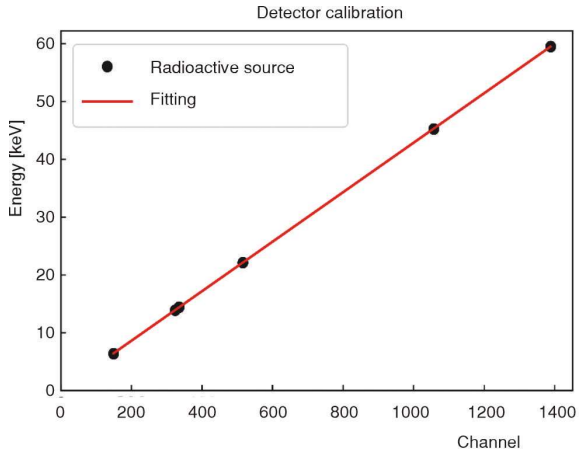


**Figure 3. Detector calibration**

lowed by applying Gaussian fitting to determine the peak channel positions for each individual energy peak. Next, a linear fit is conducted using six selected energy points to establish a functional relationship between the detector's energy and the corresponding channel addresses. This step is crucial for determining the energy linearity of the HPGe detector.

Based on the data presented in tab. 2, six energy points from the radioactive source were selected to perform a linear fit between the channel addresses and the corresponding energies, thereby establishing the linear relationship between the energy and channel address for the HPGe detector. The results of this fitting are depicted in fig. 3. Consequently, the energy linearity equation for the HPGe detector is $E = 0.0428 \cdot h + 0.0434$

In the equation, $E$ represents the X-ray energy, while ch denotes the center channel address of the single-energy peak after fitting; the intercept of the linear relationship is 0.0434.

This study adopted the transmission method to measure the mass attenuation coefficient of the samples. The transmission method is the most widely used and convenient experimental method for measuring the mass attenuation coefficient of materials [37]. When radiation is allowed to pass through any material, its intensity gradually decreases due to interactions between the radiation and atoms in the attenuating medium, causing the absorption and scattering of the original photons. Specifically, when monochromatic X-rays pass through a sample, their intensity decreases exponentially with the thickness of the sample according to the Beer-Lambert law. By measuring the intensity of X-rays before and after transmission, the mass attenuation coefficient can be calculated. Moreover, to improve measurement accuracy, this paper also considered parameters such as the density, mass, and area of the sample. By ensuring that X-rays meet the conditions of *single-energy* and *narrow beam*, when monochromatic X-rays pass through a material with a mass thickness of $x$, they interact with the material. According to the Beer-Lambert rule, eq. 1 determines how the photon attenuation intensity decreases exponentially [38]

$$\frac{I}{I_0} = \exp\left(-\frac{\mu}{\rho}x\right) \tag{1}$$

Photon intensity decreases from $I_0$ to $I$, and the mass thickness $x$ is defined as the mass per unit area, that is, $x = \rho t$, where $\rho$ is the material's density and $t$ is the material's thickness. The mass attenuation coefficient is denoted by $\mu/\rho$ with units of cm$^2$g$^{-1}$. Equation (1) can be rewritten based on empirical data of $I_0$, $I$, and $x$ [39]

$$\frac{\mu}{\rho} = \frac{1}{x}\ln\frac{I_0}{I} \tag{2}$$

Measuring the thickness of materials at the micrometer level can be challenging, and there tends to be a significant deviation in thickness during sample preparation. However, the mass $M$ and area $A$ of the sample hold more advantages in measurement and analysis. Therefore, the formula can be rewritten as [40]

$$\frac{\mu}{\rho} = \left(\frac{M}{A}\right)^{-1}\ln\frac{I_0}{I} \tag{3}$$

## RESULTS AND ANALYSIS

The typical X-ray energy spectra for directly incident beams and beams transmitted through the absorber are shown in fig. 3 and fig. 4, with a counting time of 200 seconds. The number of photons studied in

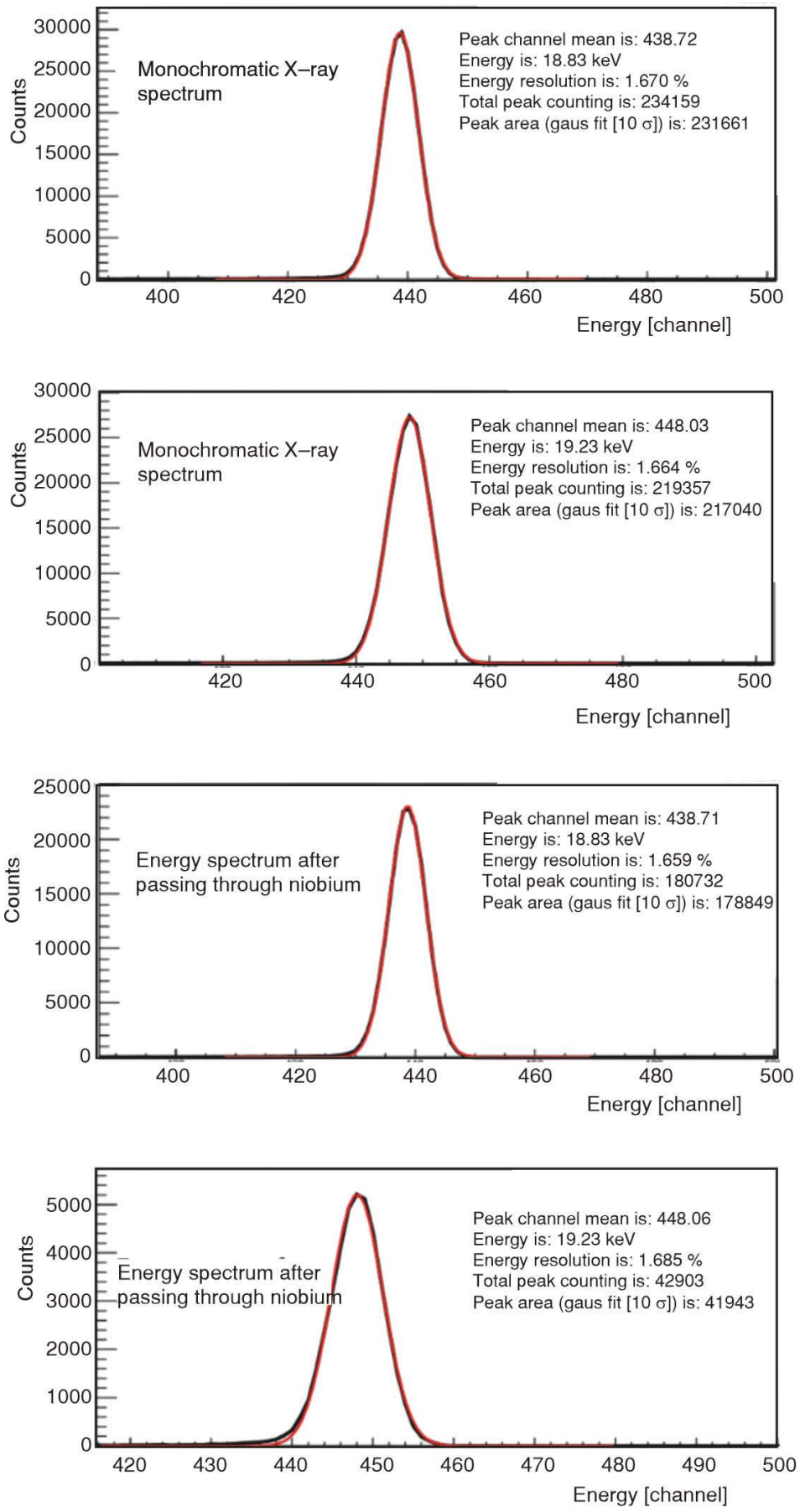


**Figure 4. Software fitting obtained typical energy spectrum diagram**

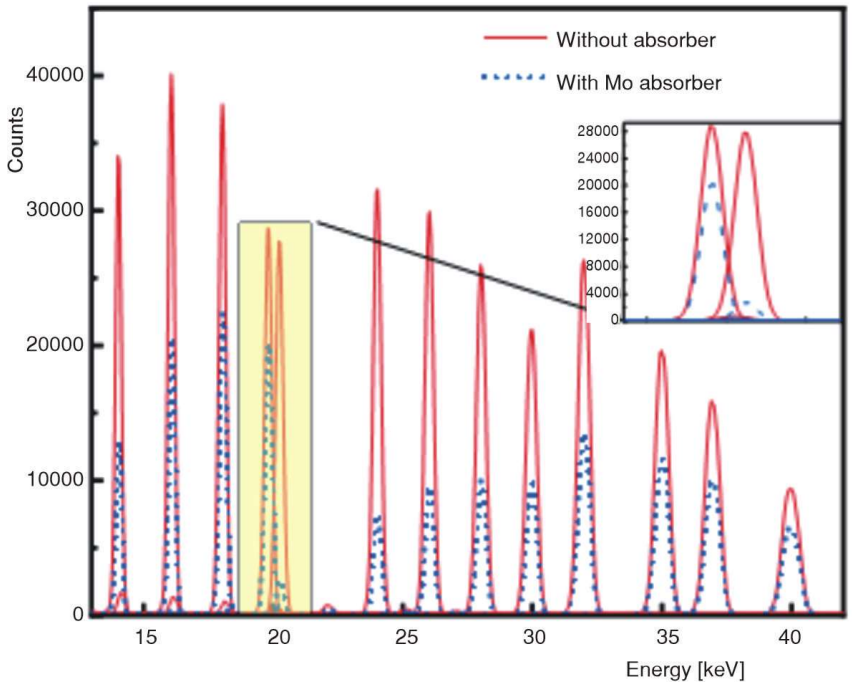


**Figure 5. Material transmission material before and after the energy spectrum (material Mo, absorption edge near 19.8-20.2 keV)**

the experiment was represented by the net peak area counts of the monochromatic X-ray peak in the spectra with and without the absorption foil. During the experiment, measurements were taken with an energy step of 0.1 keV near the K-edge and pre-edge regions, with the step size increasing to 1 keV as the distance from the theoretical K-edge increases. As seen in the fitted energy spectra in fig. 3, a clear monochromatic peak is visible. The energy points of the monochromatic peaks in the spectra with and without material transmission are the same, as shown in fig. 5. However, only the peak area counts before and after transmission change significantly. This indicates that the energy points of the monochromatic peaks are not affected by any materials. From the decrease in the height of the monochromatic peak, it can be observed that at the same energy point, the peak area counts decrease significantly after material shielding, especially for low-energy photons and photons near the absorption edge. Therefore, for the study near the absorption edge, it is necessary to use thinner metal foils, with the L-absorption limit requiring foils thinner than 1 μm.

The experimental and simulated mass attenuation coefficient curves for the four materials were plotted and compared with the values from NIST-XCOM, Phy-x, and NIST-FFAST, as shown in fig. 6. It can be observed that the curves for the four materials are generally consistent with the theoretical curves.

Figure 6(a) presents the measured values of the mass attenuation coefficient for Nb, with the photon energy range covering 8-40 keV. It can be seen that the experimental values for Nb are more consistent with the XCOM theory, with the relative deviation from the NIST-XCOM theoretical values being less than 27.5 %. This is primarily due to the complex structure of the Nb

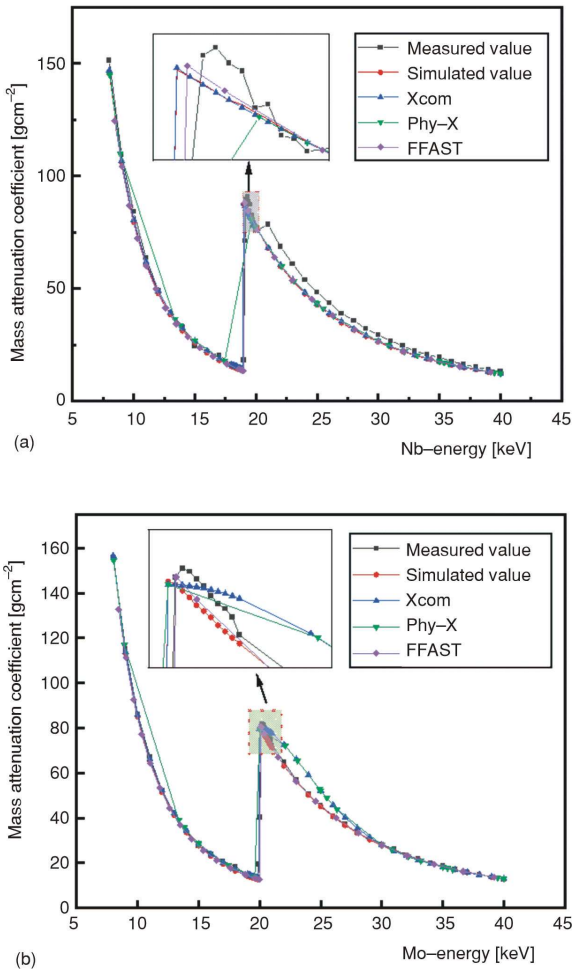


**Figure 6. The measured values of four elemental elements and the curve of theoretical mass attenuation coefficient**

absorption edge, which reflects the fine structure of Nb atoms with different atomic states. Additionally, the deviation is only significant near the absorption edge at 18.9-19 keV due to the drift of the device energy points. The measurement values are generally lower than the XCOM theoretical values, and the phy-x program obtained discontinuous data near the Nb absorption edge, resulting in a large deviation in the depicted curve. Therefore, the phy-x data are not considered as a reference in the subsequent deviation analysis.

Figure 6(b) shows the measured values of the mass attenuation coefficient for Mo, with the photon energy range covering 8-40 keV. It can be observed that the measurement values at the absorption edge front are in good agreement with the simulated and theoretical values from the reference database, with the relative deviation from the NIST-XCOM theoretical values being less than 49.3 %. Among them, the agreement with FFAST is better at the absorption edge trailing edge, while the deviation from the NIST--XCOM theoretical values increases. As the energy point moves away from the absorption edge, the consistency between the measurement and theoretical values improves.

Figure 6(c) and fig. 6(d) present the measured values of the mass attenuation coefficient for Ta and W, with the photon energy ranges covering 40-80 keV. It can be seen that the relative deviation from the NIST-XCOM theoretical values is less than 20 % for Ta and less than 17.1 % for W. The error also gradually decreases as the photon energy moves away from the K-edge.

The presence of edge effects results in deviations of the experimental values from the theoretical values when photons approach the K-shell binding energy. Firstly, the experimental results reflect the state of the atoms near the absorption edge of the samples, while the theoretical values only provide a general trend. From the comparison of the four materials, it is evident that the overall trend of the measured energy range is basically consistent. Secondly, factors affecting the measured values include thickness non-uniformity of the samples, fluctuations in the X-ray intensity during the experiment, photon counting statistical errors, and peak area calculations. Reducing the sample thickness can increase the count, or enhancing the intensity of the monochromatic X-ray can also improve the measurement accuracy. High energy resolution detectors can further improve the measurement precision of the mass attenuation coefficient [41]. Based on the measurement results, the K-shell jump ratio $r_K$ and the jump factor $J_K$ can be calculated using the following formulas [42]

$$r_K = \frac{\left(\frac{\mu}{\rho}\right)_{top}}{\left(\frac{\mu}{\rho}\right)_{bottom}} \tag{4}$$

where, $r_K$ represents the K-shell jump ratio, $(\mu/\rho)_{top}$ is the maximum measured value of the mass attenuation coefficient, and $(\mu/\rho)_{bottom}$ is the minimum measured value of the mass attenuation coefficient. After obtaining the K-shell jump ratio, the jump factor ($J_K$) can be calculated using the formula [43]

$$J_K = \frac{r_K - 1}{r_K} \tag{5}$$

The measured values of the K-shell jump ratio and the jump factor are presented in tab. 2.

The tab. 3 presents the K-edge jump ratio and jump factor obtained from the experiment, compared with values from other published databases. The relative deviations are calculated as [44]

$$\frac{\Delta r_K}{r_K} = \frac{r_{K,EXP} - r_{K,DB}}{r_{K,DB}} \times 100[\%] \tag{6}$$

In the eq. (4), EXP represents the experimental K-edge jump ratio for the material, while DB denotes values from published databases. According to tab. 3 and eq. (5), the relative deviations of the measured and calculated K-edge jump ratio for Nb material compared to GEANT4 simulation values, NIST-XCOM, and NIST-FFAST database theoretical values are 2.22 %, 3.35 %, and 2.22 %, respectively. For Mo material, the deviations are 2.27 %, 4.63 %, and 1.58 %, respectively. For Ta materia l, the deviations are 4.29 %, 8.46 %, and 9.2 %, respectively. For W material, the deviations are 22.5 %, 19.4 %, and 23.9 %, respectively.

The relative deviations of the measured and calculated K-edge jump factor for Nb material compared to GEANT4 simulation values, NIST-XCOM, and NIST-FFAST database theoretical values are 0.355 %, 0.6 %, and 0.356 %, respectively. For Mo material, the deviations are 0.35 %, 0.96 %, and 0.238 %, respectively. For Ta material, the deviations are 1.44 %, 2.71 %, and 2.79 %, respectively. For W material, the deviations are 8.2 %, 7.12 %, and 7.67 %, respectively.

The mass attenuation coefficient varies with photon energy and is independent of density and spe-

**Table 3. The K-edge jump ratio and jump factor**

| Methods | Nb | | Mo | | Ta | | W | |
|---|---|---|---|---|---|---|---|---|
| | $r_K$ | $J_K$ | $r_K$ | $J_K$ | $r_K$ | $J_K$ | $r_K$ | $J_K$ |
| Experimental | 6.362 | 0.843 | 6.282 | 0.841 | 4.056 | 0.753 | 3.535 | 0.717 |
| XCOM | 6.156 | 0.838 | 6.004 | 0.833 | 4.431 | 0.774 | 4.385 | 0.772 |
| Simulated | 6.503 | 0.846 | 6.428 | 0.844 | 4.238 | 0.764 | 4.562 | 0.781 |
| FFAST | 6.503 | 0.846 | 6.381 | 0.843 | 4.432 | 0.774 | 4.381 | 0.772 |

cific to the material [45]. Since the parameters in eq. (2) are measured independently, the uncertainty is mainly determined by the sample characteristics and beam intensity. Therefore, the uncertainty of the measured mass attenation coefficient is determined by [46]

$$\frac{u\left(\frac{\mu}{\rho}\right)}{\frac{\mu}{\rho}}=\sqrt{\left(\frac{u(A)}{A}\right)^2+\left(\frac{u(M)}{M}\right)^2+\left(\frac{u(I)}{I}\right)^2+\left(\frac{u(I_0)}{I_0}\right)^2} \quad (5)$$

The obtained synthetic relative uncertainty is ≤2.7 %, the results show that the trend of the measurement calculation values is consistent with the theoretical value curve of the database, the data fits well, and the deviation and uncertainty are within an acceptable range.

## CONCLUSION

In the present study, we successfully measured the mass attenuation coefficients of niobium, molybdenum, tantalum, and tungsten at various photon energies through experimentation, and conducted a comparative analysis with theoretical values. The findings indicate that the experimental data are largely consistent with theoretical predictions, with relative deviations falling within an acceptable range. This validates the efficacy and reliability of the single-energy X-ray radiation apparatus for the measurement of mass attenuation coefficients.

## ACKNOWLEDGMENT

The following appreciation is expressed to the staff of Division of Ionizing Radiation Metrology, National Institute of Metrology (NIM) of China which offers a great help in the phase of development. The authors declare that they have no known competing financial interests or personal relationships that could have appeared to influence the work reported in this paper. This work was supported by the National Natural Science Foundation of China(No.12205289), the NQI project (2023YFC2206502) and project(AKYZ D2412).

## AUTHORS' CONTRIBUTIONS

The manuscript is written by Z. Wang and Z. Shu. Review and discussion by S. Guo, X. Zhou, Z. Li, S. Huang and J. Wu. All authors participated in the preparation of the final version of the manuscript.

## ORCID NO

Zhen Wang: 0009-0007-6642-8607

## REFERENCES

[1] Osman, A. F., *et al.*, Effect of PbO Incorporation With Different Particle Size on X-Ray Attenuation of Polystyrene, *Nucl Technol Radiat, 37* (2022), 1, pp. 18-30
[2] Li, H., *et al*., Flexible and Wearable Functional Materials for Ionizing Radiation Protection: A Perspective Review, *Chemical Engineering Journal, 487* (2024), 150583
[3] More, C. V., *et al*., Polymeric Composite Materials for Radiation Shielding: A Review, *Environmental Chemistry Letters, 19* (2021), pp. 2057-2090
[4] Sepideh, Y. D., *et al*., Studies on Mass Attenuation Coefficients for Some Body Tissues with Different Medical Sources and Their Validation Using Monte Carlo codes, *Nuclear Science and Techniques, 31* (2020), 12, pp. 50-64
[5] Ma, D., *et al*., Mechanical and Medical Imaging Properties of 3D-Printed Materials as Tissue Equivalent Materials, *Journal of Applied Clinical Medical Physics, 23* (2022), e13495
[6] Barba-Lobo, A., *et al*., A General Function for Determining Mass Attenuation Coefficients to Correct Self-Absorption Effects in Samples Measured by Gamma Spectrometry, *Radiation Physics and Chemistry, 179* (2021), 109247
[7] Tekin, Huseyin, O., MCNP-X Monte Carlo Code Application for Mass Attenuation Coefficients of Concrete at Different Energies by Modeling 3 × 3 Inch NaI(Tl) Detector and Comparison with XCOM and Monte Carlo Data, *Science and Technology of Nuclear Installations, 1* (2016), pp. 6547318.1-6547318.1
[8] Wang, Bo., *et al*., Monte-Carlo Simulation of Wall Correction Factor of Graphite Cavity Ionisation Chamber, *Journal of Engineering-JOE, 2019* (2019), 23, pp. 8658-8661
[9] Akman, F., *et al*., Study of Absorption Parameters Around the K Edge for Selected Compounds of Gd, *X-Ray Spectrometry, 45* (2016), 2, pp. 103-110
[10] Badawi, M. S., *et al*., Analytical Computation Technique for Calculation the Effective Geometrical Solid Angle and the Efficiency of Cubic Scintillation Crystal with Side Cylindrical Hole, *Nucl Technol Radiat, 37* (2022), 2, pp. 91-102
[11] Menesguen, Yr., *et al*., Mass Attenuation Coefficients in the Range, K Fluorescence Yield and Relative X-Ray Emission Rate for Ti, V, Fe, Co, Ni, Cu, and Zn Measured with a Tunable Monochromatic X-Ray Source, *Nuclear Instruments & Methods in Physics Research Section B, 268* (2010), 16, pp. 2477-2486
[12] Barba-Lobo, A., *et al*., A General Function for Determining Mass Attenuation Coefficients to Correct Self-Absorption Effects in Samples Measured by Gamma Spectrometry, *Radiation Physics and Chemistry, 179* (2021), 109247
[13] Shu, Z., *et al*., Measurement of Mass Attenuation Coefficients Based on Monochromatic X-Ray Radiation Devices, *Proceedings*, IEEE 16th International Conference on Electronic Measurement and Instruments, Harbin, China, 2023, pp. 68-71
[14] Xing, Z., *et al*., Establishment and Study of a Polarized X-Ray Radiation Facility, *Nuclear Science and Techniques, 34* (2023), 8, pp. 54-63
[15] Shuo, Z., *et al*., Transition Edge Sensor-Based Detector:from X-ray to $\gamma$-Ray, Nuclear Science and Techniques, 33 (2022), 7, pp. 61-72
[16] Fan, Li,, *et al*., Absolute Measurement of Radiant Power for Synchrotron Radiation Monochromatized X-Rays, *Radiation Detection Technology and Methods, 4* (2020), 1, pp. 97-105

[17] Yu, T., *et al.*, Research on the Temperature Characteristics of SiPM-Based LaBr3(Ce) Detectors, *Journal of the Korean Physical Society, 82* (2023), 1, pp. 12-18
[18] Huang, S., *et al*., Research on the Energy Response of Monochromatic X-Ray in (3-40) keV, *IET Conference Proceedings, 2022* (2022), 18, pp. 275-279
[19] Guo, S., *et al*., Research on a Tunable Monochromatic X-Rays Source in (5~40) keV, *Applied Radiation and Isotopes, 181* (2022), 110096
[20] Li, M., *et al*., Study on the Performance of X-Ray Machines Used in K-Fluorescent Devices, *Journal of Engineering-JOE, 2019* (2019), 23, pp. 8781-8785
[21] Kumar, A. M., *et al*., Measurement of Mass Attenuation Coefficient of ZIRCONIUM (Zr), Zirconium Chloride (ZrCl4) and Zirconium Silicate (ZrSiO4) Near the K-Edge Using Synchrotron Radiation, *Materials Today: Proceedings, 38* (2021), 5, pp. 2927-2934
[22] Menesguen, Y., *et al.*, High Accuracy Experimental Determination of Copper and Zinc Mass Attenuation Coefficients in the 100 eV to 30 keV Photon Energy Range, *Metrologia, 53* (2016), 1, pp. 7-17
[23] Menesguen, Y., *et al.*, Experimental Determination of L Fluorescence Yields of Gadolinium, *X-Ray Spectrometry, 49* (2020), 5, pp. 596-602
[24] Menesguen, Y., *et al*., Advances in the Measurements of the Mass Attenuation Coefficients, *X-Ray Spectrometry, 48* (2019), 5, pp. 330-335
[25] Thabet, A. A., *et al*., Study of Mathematical Functions to Fit Detector Efficiency Curve in Gamma Ray Energy Range From 59.54 keV Up to 1408.01 keV, *Nucl Technol Radiat, 36* (2021), 3, pp. 224-233
[26] Abbas, Y. M., *et al*., Gamma Attenuation Through Nano Lead – Nano Copper PVC Composites, *Nucl Technol Radiat, 36* (2021), 1, pp. 50-59
[27] Alharshan, G. A., *et al*., A Comparative Study Between Nano-Cadmium Oxide and Lead Oxide Reinforced in High Density Polyethylene as Gamma Rays Shielding Composites, *Nucl Technol Radiat, 35* (2020), 1, pp. 42-49
[28] More, C. V., *et al*., Extensive Theoretical Study of Gamma-Ray Shielding Parameters Using Epoxy Resin-Metal Chloride Mixtures, *Nucl Technol Radiat, 35* (2020), 2, pp. 138-149
[29] Alsayed, Z., *et al*., Study of Some Gamma Ray Attenuation Parameters for New Shielding Materials Composed of Nano ZnO Blended with High Density Polyethylene, *Nucl Technol Radiat, 4* (2020), 4, pp. 342-352
[30] Badawi, M. S., A Numerical Simulation Method for Calculation of Linear Attenuation Coefficients of Unidentified Sample Materials in Routine Gamma Ray Spectrometry, *Nucl Technol Radiat, 4* (2016), 4, pp. 249-259
[31] Pengyue, Z., *et al*., Research on High-Energy Performance of GECAM Satellite GRD Detector, 14th IEEE International Conference on Electronic Measurement & Instruments (ICEMI), IEEE, *Proceedings*, 2019, DOI:10.1109/ICEMI46757.2019.9101670
[32] Siming, G., *et al.*, Measurement of Air Attenuation and Recombination Correction Factors in Synchrotron Radiation X-Rays, *Proceedings*, 14th IEEE International Conference on Electronic Measurements & Instrumentations (ICEMI), Changsha, China, May 2019
[33] Si-Ming, G., *et al*., The Development, Performances and Applications of the Monochromatic X-Rays Facilities in (0.218-301) keV at NIM, China, *Nuclear Science and Techniques, 32* (2021), 6, pp. 108-121
[34] Hou, D., *et al*., The Realization and Study of (21-301) keV Monochromatic X-Rays, *Nuclear Instruments & Methods in Physics Research Section A-Accelerators Spectrometers Detectors and Associated Equipment, 927* (2019), May, pp. 382-389
[35] Obeid, A., *et al*., Effects of Different Nano Size and Bulk WO3 Enriched by HDPE Composites on Attenuation of the X-Ray Narrow Spectrum, *Nucl Technol Radiat, 36* (2021), 4, pp. 315-328
[36] Li, M., *et al*., Realisation and Measurement of (6-15) keV Single-Energy X-Rays, *The Journal of Engineering, 2019* (2019), 23, pp. 8662-8666
[37] Guo, S., *et al*., Study on Silicon Drift Detector Efficiency Using Monte-Carlo Simulation and Experimental Methods, *The Journal of Engineering, 2019* (2019), 23, pp. 8543-8545
[38] Gupta, M. K., *et al*., Measurement of Absorption Edge Parameters Near K Edge for the Compounds of Zn, Zr, Cd, Ba, and Pb, *Journal of Alloys and Compounds, 623* (2015), pp. 407-412
[39] Guo, K. Y., *et al*., Mass Attenuation Coefficient of Medical Radiation Module Measured by HXCF, *Journal of Metrology, 44* (2023), 4, pp. 616-621
[40] Akman, F. D., *et al.*, Studies on Effective Atomic Numbers, Electron Densities from Mass Attenuation Coefficients Near the K Edge in Some Samarium Compounds, *Applied Radiation and Isotopes, 101* (2015), 1, pp. 107-113
[41] Guo, S., *et al*., Design and Verification of a Radiation Detector's Electronics System, *The Journal of Engineering, 2019* (2019), 23, pp. 8527-8530
[42] Uzunoglu, Z., Determination of Absorption and Shielding Parameters for $Ba(ClO_4)_2.3H_2O$ Using Experimental and Theoretical Methods, *Radiation Physics and Chemistry, 212* (2023), 111090
[43] Roy, B. R., *et al*., Measurement of X-Ray Mass Attenuation Coefficient of Nickel Around the K-Edge Using Synchrotron Radiation Based X-Ray Absorption Study, *Radiation Physics and Chemistry, 114* (2015), Sept., pp. 38-42
[44] Guo, S., *et al*., Study on the Correction Method for the Dead-Time Effects of Neutron Detectors Due to Pulsed Radiation, *Journal of the Korean Physical Society, 72* (2018), 4, pp. 485-491
[45] Menesguen, Y., *et al*., Advances in the Measurements of the Mass Attenuation Coefficients, *X-Ray Spectrometry, 48* (2019), 5, pp. 330-335

Received on June 25, 2024
Accepted on September 9, 2024

**Џен ВАНГ, Симинг ГУО, Цијао ШУ, Синг ЏОУ, Цивеј ЛИ, Шикуеј ХУАНГ, Ђинде ВУ**

## МЕРЕЊЕ МАСЕНОГ КОЕФИЦИЈЕНАТА СЛАБЉЕЊА НИОБИЈУМА, МОЛИБДЕНА, ТАНТАЛА И ВОЛФРАМА У БЛИЗИНИ ГРАНИЦЕ АПСОРПЦИЈЕ

Овај рад користи уређај за монохроматско рендгенско зрачење који је успоставио Национални институт за метрологију у Кини, да спроведе систематско експериментално истраживање масеног коефицијената слабљења метала ниобијума, молибдена, тантала и волфрама у близини њихових K апсорпционих граница. Способност уређаја да генерише континуално подесиве монохроматске рендгенске зраке и прецизно мери број фотона, пружа идеалан услов за прецизна мерења масеног коефицијената слабљења. У раду је коришћен минимални енергетски корак од 0.1 keV да би се систематски добио количник скока (rK) и фактор скока (JK) у близини K ивица апсорпције четири материјала. Експериментална мерења упоређена су са теоријским вредностима из база података NIST-XCOM, NIST-FFAST и Phy-x, показујући конзистентан тренд између експерименталних и теоријских резултата, са релативним одступањима у прихватљивим границама, чиме се потврђује поузданост теоријских модела. Анализа несигурности открива комбиновану релативну несигурност мању од 2.7 %, што указује да су експериментални резултати и теоријске вредности у добром слагању, са одступањима и несигурностима унутар прихватљивих опсега. Ово истраживање даје значајне експерименталне податке и теоријске референце за примену уређаја за монохроматско рендгенско зрачење у области мерења масеног коефицијената слабљења.

*Кључне речи: масени коефицијент слабљења, граница апсорпције, монохроматско рендгенско зрачење, количник скока, фактор скока*